Soft Matter

Structural and Rheological Aging in Model Attraction-Driven Glasses by Rheo-SANS

Journal:	*Soft Matter*
Manuscript ID	SM-ART-07-2020-001373.R1
Article Type:	Paper
Date Submitted by the Author:	31-Oct-2020
Complete List of Authors:	Gordon, Melissa; Lafayette College, Department of Chemical and Biomolecular Engineering; University of Delaware, Department of Chemical and Biomolecular Engineering Kloxin, Christopher; University of Delaware, Materials Science and Engineering; University of Delaware, Chemical and Biomolecular Engineering Wagner, Norman; University of Delaware, Chemical Engineering

Structural and Rheological Aging in Model Attraction-Driven Glasses by Rheo-SANS

Melissa B. Gordon[1,2], Christopher J. Kloxin[2,3], Norman J. Wagner[2]*

[1]Department of Chemical and Biomolecular Engineering, Lafayette College, 740 High Street, Easton, PA 18042, USA
[2]Department of Chemical and Biomolecular Engineering, Center for Neutron Scattering, University of Delaware, 150 Academy Street, Newark, DE 19716, USA
[3]Department of Material Science and Engineering, Center for Neutron Science, University of Delaware, 201 DuPont Hall, Newark, DE 19716, USA

* Corresponding Author, Email: wagnernj@udel.edu

Keywords: colloidal glasses, aging, glass microstructure, thermoreversible interactions, adhesive hard spheres

Abstract

Aging in a model colloidal suspension comprised of particles with a thermoreversible attraction is studied using Rheo-SANS techniques in the attractive-driven glass state. Multiple thermal pathways lead to a common rheological and microstructural aging trajectory, as was observed previously for a thermoreversible gel. SANS measurements of the colloidal glass microstructure as a function of temperature and time during various quench protocols are quantitatively characterized in terms of an effective interaction strength that becomes an order parameter defining the microstructural state of the glass. Using previously validated concepts of a fictive temperature, a semi-empirical, quantitative relationship similar to an Avrami relationship is established between the mechanical aging (elastic modulus) and microstructural aging (order parameter) that is independent of thermal history for the thermal profiles studied herein at long times. Furthermore, shear rejuvenation is studied, and while shear may only partially reduce the degree of structure in the glass, aging upon flow cessation is found to follow a common trajectory when viewed in terms of the microstructural order parameter.

I. Introduction

The study of out-of-equilibrium systems is of fundamental scientific interest and industrial applicability, and therefore characterizing and controlling these systems is considered by the Department of Energy as one of the five grand challenges facing scientists today [1]. Colloidal dispersions are usually out-of-equilibrium systems that are of particular relevance as they are found in a wide variety of natural and synthetic consumer products, such as foods, pharmaceuticals, paints and cosmetics [2]. Moreover, colloidal dispersions are often employed as model systems to probe and understand non-equilibrium behavior in other materials of interest, such as atomic or molecular systems, because colloidal dispersions have more experimentally accessible length scales and timescales [3]. In particular, the upper size scale of colloidal particles allows for the tracking of the motion of micron-sized particles using optical microscopy [4, 5]. Additionally, the use of colloidal glasses to understand behavior in structural glasses is particularly advantageous as the volume fraction can be easily altered in colloidal glasses, while the effects of density and temperature are coupled in molecular glasses [6]. Furthermore, the

tunable interactions between colloidal particles and ability to purchase or synthesize particles of varying shapes and sizes also contribute to their utility as models to understand other condensed matter systems and yield stress fluids more broadly [7]. More about the physics of colloidal glasses and gels and their rheology can be found in a recent book chapter [8].

Aging phenomena are observed in many types of glassy colloidal dispersions [2, 9, 10]. Specifically, colloidal dispersions are often observed to be in dynamically arrested states with significantly hindered mobility, which prevents the system from reaching thermodynamic equilibrium on experimental timescales [2, 11-13]. However, sufficient thermal mobility of the colloidal particles enables the system to evolve toward thermodynamic equilibrium on an experimental timescale; for example, the aging behavior in model colloidal glass systems, such as Laponite [6, 14-18], star polymers [19, 20] and colloid-polymer mixtures [21-23] have been observed in both experiments and simulations. In this context, the "age" of the sample refers to the time elapsed since the material was rejuvenated, where rejuvenation is a mechanical or thermal process that erases the structural history of the sample before a new test is conducted. Typically, as the sample ages, the rate of aging decreases and the relaxation time of the material increases [9]. This time-dependent behavior complicates the characterization of these aging systems, which is required to accurately report, control, and predict product stability, shelf-life, and safety. Residual stresses after processing or flow are also implicated [24].

Importantly, the mechanism underlying the aging process may be specific to the evolution of a particular microstructure in the system. Stiakakis et al.[25] used multispeckle dynamic light scattering (MSDLS) and small angle neutron scattering (SANS) to determine that multi-arm star polymer glasses age via crystallization, which resulted in an increased rate of the short-time diffusion. Pham and coworkers[21] mapped the transition from a repulsive to attractive glass in a colloidal glass formed through depletion interactions and noted aging effects in all non-crystallizing samples; static light scattering was used to probe the underlying structure yet, within the attractive glasses of varied attraction strength, structural changes could not be resolved. To correlate the dynamics to structure during aging, Cianci et al.[26] used a glassy system composed of poly(methyl methacrylate) (PMMA) colloids in a mixture of decalin and cyclohexylbromide and monitored the real-time motion using confocal microscopy. While they did not determine a mechanism, their results suggested a correlation between structure and dynamics during aging; tetrahedra that are categorized as "looser" and more "irregular" led to enhanced mobility that facilitated the aging process. Additionally, computer simulations of aging attractive colloidal glasses conducted by the Cates group showed that the number of bonds per particle increases as the system aged, resulting in a stiffer network that relaxed more slowly [27]. Overall, these results highlight the complex behavior associated with aging in colloidal glasses and emphasize the importance of uncovering its mechanistic origin and exploring its structural evolution.

Applied stress may alter the aging process, and these results are typically interpreted in the context of the free energy landscape viewpoint of colloidal aging. Briefly, this viewpoint describes a complex landscape of free energy states in which the system continuously explores and evolves toward lower free energy via thermal motion, resulting in continuous aging [28-30]. This aging can be accelerated or even rejuvenated by shear. For example, Viasnoff et al. [31] measured the relaxation dynamics in a glassy suspension of polybeads and showed that high shear and low shear led to rejuvenation and "overaging," respectively, where overaging refers to accelerated aging. To interpret their bulk measurements, they proposed that on a microscopic level the high strain destabilized the glass (melted), while moderate strains enabled the sample to explore more stable glassy configurations. Simulations, such as those by Lacks and Osborne[32] qualitatively corroborate the experimental results of Viasnoff et al. [31] Using an energy landscape framework, they reported that a cycle of large strain rejuvenated the glass while a small strain resulted in overaging (i.e., shear "shuffled"), enabling the system to reach shallower or deeper energy minima, respectively. While computer simulations have been performed to help understand aging phenomena [33], experimental measurements of the microstructure of a colloidal glass during such rejuvenation and overaging is lacking.

Here, we examine the structural basis of the rejuvenation and overaging phenomenon by directly measuring the effect of shear on the colloidal glass microstructure via time-resolved SANS techniques [34]. Moreover, by using a system that is fully rejuvenated by thermal cycling, we thoroughly investigate the use of shear as a rejuvenation method, which may fully regenerate the original mechanical properties, but incompletely rejuvenate the microstructure [35]. We employ a well-characterized model colloidal suspension of nanoscale, thermoreversible adhesive hard sphere (AHS) particles that are comprised of octadecyl-functionalized nanoparticles dispersed in tetradecane [36-39]. The attractive potential of this AHS system has been previously described [37] and, at the volume fraction selected for this study (ϕ=0.46), the system forms an attraction-driven glass (ADG). The attractive interactions are controlled by temperature, which induces a phase transition of the octadecyl brush [40]. At 40°C, the sample melts and is subsequently subjected to a pre-shear protocol that fully erases the structural history. Rheological aging in the gel state was first observed in this system by Eberle et al. [36], who proposed aging occurred via the interdigitation of the brush. In the same colloidal gel system, our recent work develops a quantitative and predictive relationship between the macroscopic properties and the underlying microstructure during gel aging, which is independent of the thermal and shear history of the gel [41]. Here, we extend this work by connecting rheological aging to structural aging in a colloidal glass through simultaneous bulk property and microstructural measurements. Moreover, we examine the effects of thermal and shear history on the glass structure and properties. Under these experimental conditions, this thermoreversible system forms a homogeneous glass and thus, exhibits a fundamentally distinct and previously unexplored aging mechanism compared to the model systems described above.

II. Experimental methods

A. Preparation of the thermoreversible AHS system

The octadecyl-coated silica nanoparticles were functionalized using an established protocol in the literature[40, 42]. Briefly, Ludox TM-50 silica nanoparticles (30 nm in diameter) were purchased from Sigma Aldrich and reacted with 1-octadecanol (Alfa Aesar). The particles were purified by centrifugation in a Sorvall RC 6 Plus centrifuge and dried under a nitrogen stream and then in a vacuum oven for at least 24 hours. Full characterization of the functionalized nanoparticles is reported elsewhere [36, 40]. The dried particles were dispersed in tetradecane at room temperature to prepare a sample with a volume fraction of 0.46 which forms a glassy, thermoreversible adhesive hard sphere (AHS) system.

B. Rheometry

Aging experiments were performed on a discovery hybrid rheometer (DHR) from TA Instruments using cone and plate geometry (40 mm cone diameter, 2° cone angle) equipped with a solvent trap and Peltier plate where there was a 1°C difference in temperature compared to the gas-cooled Rheo-SANS environment used below. Specimens were subjected to a pre-shear protocol in which the sample was sheared for 2 minutes at a rate of 10 s^{-1} in its liquid state at 40°C and then held quiescently at 40°C for an additional 2 minutes. Soft glass formation and aging were monitored using small oscillatory shear measurements at 0.1% strain and a frequency of 1 rad/s as the sample was quenched from 40°C to 28.4°C and aged isothermally at 28.4°C.

C. Small-angle neutron scattering (SANS)

Static SANS measurements were also conducted at the NIST NCNR on the NCB 30 m beamline. Detector distances of 1 m, 4 m, 13 m (with and without a focusing lens) were used. Samples were loaded into cells with 0.01-inch aluminum spacers such that sample transmissions were approximately 0.80, thereby mitigating multiple scattering effects. The cells were loaded into a 10-position sample holder (10CB) equipped with a fluid bath to maintain the set temperature throughout the experiment. Samples were equilibrated at the desired temperature for at least 20 minutes prior to measurement.

D. Concurrent rheological and structural measurements (Rheo-SANS)

Simultaneous rheological measurements and small angle neutron scattering (Rheo-SANS) were conducted at the National Institute of Standards and Technology (NIST) Center for Neutron Research (NCNR) in Gaithersburg, MD using the Rheo-SANS sample environment [43]. Time-resolved SANS experiments were performed on the NGB 30m beamline in the 1-3 (shear, vorticity) plane at a detector distance of 13 m with a focusing lens. An Anton Paar MCR-501

stress-controlled rheometer was placed into the beamline and the AHS sample was contained within titanium concentric cylinder geometry with an inner bob diameter of 28 mm and a 0.5 mm gap. The total sample path-length was 1 mm and sample transmissions ranged from 0.301 to 0.304. Between experiments, the sample was rejuvenated using a two-step pre-shear protocol in which the sample was (1) sheared in its liquid state at 10 s^{-1} for 10 minutes at 40°C and (2) held quiescently at 40°C for 2 minutes. Aging experiments were conducted at 29.4°C at 0.1% strain and a frequency of 1 rad/s. Two thermal histories were investigated: (1) the cooling direction in which the sample is quenched from its liquid state at 40°C to 29.4°C and (2) the heating direction in which the sample is quenched from 40°C to 25°C and then to 29.4°C. The gas-cooled Rheo-SANS Couette sample environment exhibited imperfect temperature control and resulted in overshoots from the set point temperature. The shear history dependence was evaluated by shearing the aged sample at shear rates of 5 s^{-1}, 100 s^{-1}, 500 s^{-1} and 1000 s^{-1}. A reference time of 4250 seconds was selected for consistency with results acquired for our earlier study investigating aging in the same system, but in the gel state (ϕ=0.28) [41].

E. Rheo-SANS data analysis

The SANS scattering data was analyzed using the SANS Data Reduction Macros in Igor Pro available from NIST [44]. Time-resolved scattering results were binned using event mode processing in Igor Pro. 1-D scattering patterns were fit to the sticky hard sphere (SHS) model (or Baxter model) to extract the Baxter parameter (τ) in SAS View. Fitting parameters are described elsewhere [40, 41]. We note that because the hard sphere structure factor calculated using the Percus-Yevick closure approximation deviates from experimental and computational results at high volume fraction, we fit the scattering length density (SLD) of the shell (SLD shell = -1.989e-06 $Å^{-2}$) to data. The perturbation parameter was fixed as $\varepsilon = 0.01$ for all cases.

III. Results and discussion

This work quantitatively connects rheological aging to structural aging in a colloidal glass by combining rheometry and time-resolved small angle neutron scattering. First, in section IIIA, the microstructure of the thermoreversible colloidal system in the liquid state at 40°C and the glass state at 25°C are measured and plotted onto the AHS phase diagram developed for this system. Then, in section IIIB, results of small amplitude frequency sweeps are used to identify an appropriate temperature to perform subsequent aging experiments. In section IIIC, concurrent rheometry and SANS experiments connect the macroscopic bulk property changes to the evolution in the underlying microstructure during glass aging using two different thermal profiles and variation in shear rates.

A. Microstructural measurements at rest

SANS data for the AHS system at 40°C and 25°C are displayed in Fig. 1. The length scales probed by these measurements range from a nanometer to ~0.5 microns. At these high particle concentrations, strong, liquid-like correlation peaks are evident, with a prominent, but broad nearest neighbor or Debye-Shearer peak along with higher order local extrema. There is a clear difference in the primary correlation peak upon quenching that is evident in the inset figure magnifying this region. Notably, the high-q and very low-q data do not change with temperature. Only very subtle differences in SANS at high q are expected due to the angstrom-level changes associated with the solidification of the alkane brush on the particle surface, as have been reported previously [40]. It should be noted that there is a temperature-independent upturn in the scattering at low q that is anomalous and has been reported previously [37]. It is not known at this time whether such behavior is an artifact, e.g., multiple scattering, or possibly associated with reports of correlated regions of infrequent cooperative dynamics that have been reported for attractive driven glasses created by polymer depletion [45].

The lines are the fits of the SHS model to the data with only single adjustable parameter, the Baxter 'sticky' parameter, τ, or strength of attraction. These values enable the positioning of the samples on the AHS state diagram (Fig. 2), which confirms the rheological observation that the high temperature state is a liquid while the quenched sample is an AHS glass [37, 46]. At this high volume fraction, the particle motion is highly constrained due to caging [46]. As expected, the model does not capture the aforementioned larger length scale artifact. Based on this SANS data, we select the scattering vector (q) range ($0.008\ Å^{-1}<q<0.5\ Å^{-1}$) for Rheo-SANS experiments.

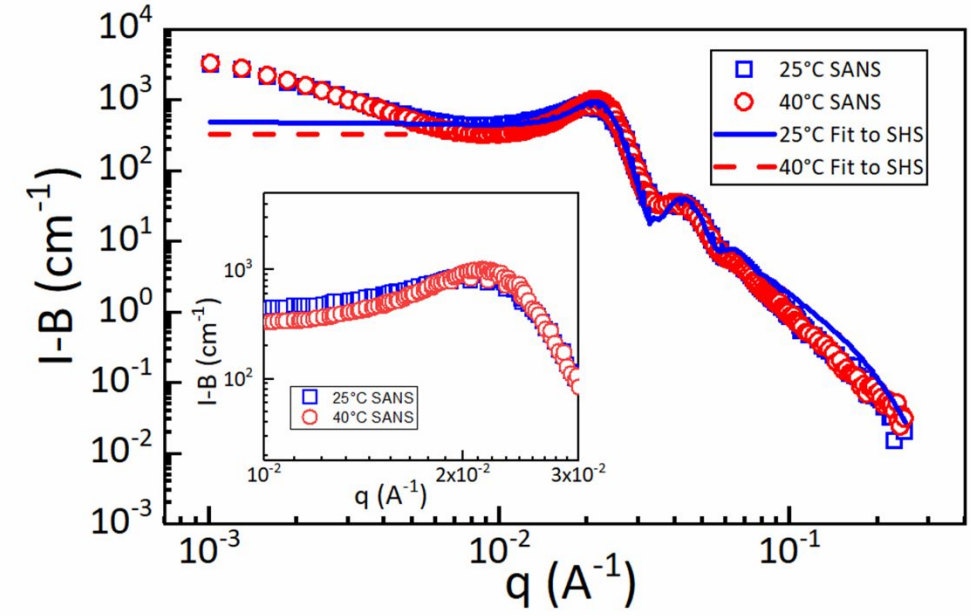

Fig 1 Small angle neutron scattering (SANS) data at 40°C (liquid state) and 25°C (glass state). The lines are the fit to the data using the SHS model, having a single adjustable parameter (i.e., the Baxter 'sticky' parameter) which are 0.367 and 0.234 at 40°C and 25°C, respectively. The inset shows the key differences around the primary peak. Note "B" is the background, which is subtracted from the overall intensity.

Fitting the microstructural measurements shown in Fig. 1 to the SHS model enables the mapping of the soft glass samples studied in this work onto the phase diagram for the AHS system (Fig. 2), [37, 46] which places these AHS glass samples in the context of previous work on the system[37, 46]. The phase diagram indicates which phases are observed as a function of the Baxter parameter (τ) and the volume fraction (ϕ). The Baxter parameter is obtained from fitting liquid state theory to scattering data, as discussed below. A lower Baxter parameter corresponds to increased interaction strength and can be thought of as an effective temperature. The (purple) arrow on the diagram points to the location of two points of interest at working volume fraction for this study (ϕ=0.46). As described explicitly later, to examine the aging process, the sample was pre-sheared in its liquid state at 40°C and is quenched to its glass state at 29.4°C where rheological and structural aging was monitored. On the phase diagram in Fig. 2, the (green) triangles represent the experimentally determined dynamic arrest transition for this system [37]. The open (red) circular marker designates the liquid state at 40°C and the (blue) square marker labels the state of the soft glass.

To analyze our data, as discussed in the methods section, we fit the data using a single parameter (SLD of the shell) to the reference state data to more carefully capture the structural changes associated with aging in the glass state. As a result, the Baxter parameter corresponding to the liquid state data obtained from this analysis appears to fall below the percolation line determined by Eberle and co-workers; however, when the SLD of the shell reported by Eberle and coworkers is used to fit the data in Fig. 1, we obtain a Baxter parameter of 1.25 (filled (red) circle on the phase diagram), which is above the experimentally determined dynamic arrest transition. For completeness, the phase diagram also contains points corresponding to the gel sample (ϕ=0.28) in the liquid state at 40°C ((red) filled circle) and in the gel state at 28.6°C ((blue) filled square), in which AHS gel aging was previously studied. [39] Overall, extracting a Baxter parameter from SHS fittings to the microstructural data locates the AHS glass samples onto the adhesive hard sphere phase diagram, which is consistent with earlier findings[37, 46].

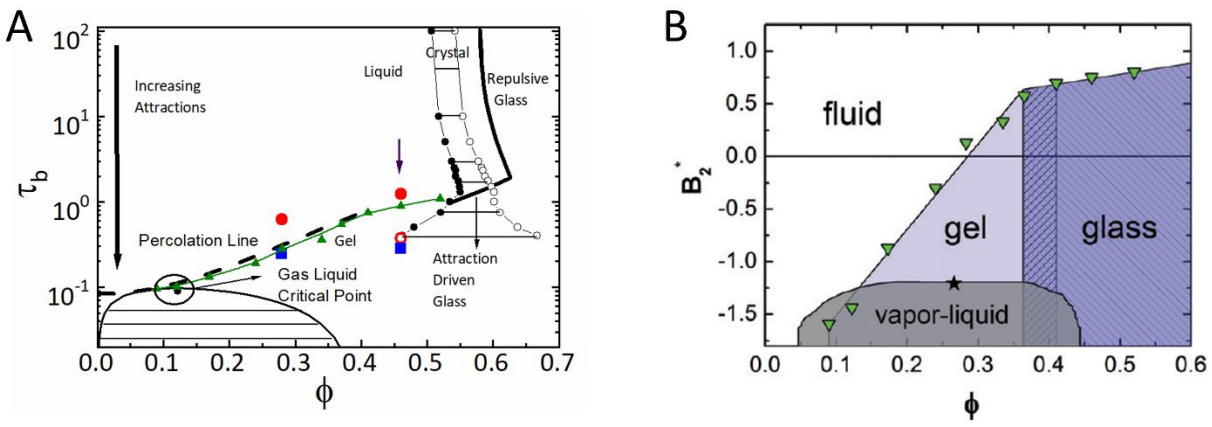

Fig 2 A. The phase diagram for the AHS system. The closed red circular marker designates the liquid state at 40°C and the closed (blue) square marker labels the aged state of the soft glass

(ϕ=0.46) and gel (ϕ=0.28) after two hours at 29.4°C and 28.6°C, respectively. The open (red) circular marker represents the liquid state using the SLD of the shell as a fitted parameter, which enabled closer fitting of the SHS model to the microstructural data during aging, but did lead to this point falling below the percolation line determined by Eberle and co-workers (experimental data shown by green triangles). Figure uses data obtained by Eberle and co-workers [37]. **B.** Universal state diagram for the second virial coefficient for the date of Eberle and co-workers (green triangles are the same experimental points) showing the transition from gel to attractive driven glass and locating this sample ϕ=0.46 in the attractive driven glass region. Reprinted with permission from (A. P. R. Eberle, R. Castaneda-Priego, J. M. Kim and N. J. Wagner, "Dynamical Arrest, Percolation, Gelation, and Glass Formation in Model Nanoparticle Dispersions with Thermoreversible Adhesive Interactions", *Langmuir*, 2012, **28**, 1866-1878) [36]. Copyright (2012) American Chemical Society.

The identification of that sample at ϕ=0.46 and low temperature as an attractive driven glass is based on the combination of caging and strength of attraction, as shown as a universal state diagram for the second virial coefficient ($B_2(T) = 1/(1 - 4/\tau_b)$). Conditions under which localization occurs and the transition from glasses to gels are discussed in detail in the extensive review by Zaccarelli [47], where a key distinguishing feature is the presence of caging for liquids above $\phi > \sim 0.4$. As discussed be Eberle et al. [36] and confirmed by simulations of Valadez et al. [46], below this volume fraction a much stronger attraction is required to dynamically arrest and the structure is necessarily more open – leading to a gel[41]. Above this volume fraction, cages exist in the liquid and the mode coupling theory can describe the transition from liquid to the attractive driven glass[48] as attractions are introduced. Interestingly, attractions can "melt" a repulsive glass to a liquid state, and then, upon further increase in strength of attractions an attractive driven glass forms [49]. Importantly, as shown in Figure 1, the very large structural peak evident at the nearest reciprocal neighbor distance identifies this sample as a highly structured liquid with significant caging such that dynamical arrest is to an attractive driven glass.

B. Rheological Measurements

Small amplitude frequency sweeps were conducted to determine the glass transition temperature and select an appropriate temperature to conduct aging experiments (Fig. 3). The sample (ϕ=0.46) was quenched from its liquid state at 40°C to the temperature indicated in Fig. 3. The sweeps in Fig. 3 indicate that the sample is highly sensitive to temperature changes as small as 0.1°C over the temperatures ranging from 29.4°C to 29.7°C. Based on this data, we observe that the transition temperature occurs between 29.5°C and 29.6°C. The line in Fig. 3 shows the expected power law behavior as described by Winter and Chambon [50]. Eberle et al. previously reported a transition temperature for the same sample (ϕ=0.46) as 30.0°C [36], and we attribute this temperature discrepancy to a slight temperature difference between the TA Instruments AR-G2 with a Peltier plate and the gas-cooled Rheo-SANS environment used in this measurement. From the frequency sweeps displayed in Fig. 3, we elected to conduct all subsequent Rheo-SANS aging experiments at 29.4°C, where a soft attraction-driven glass is observed.

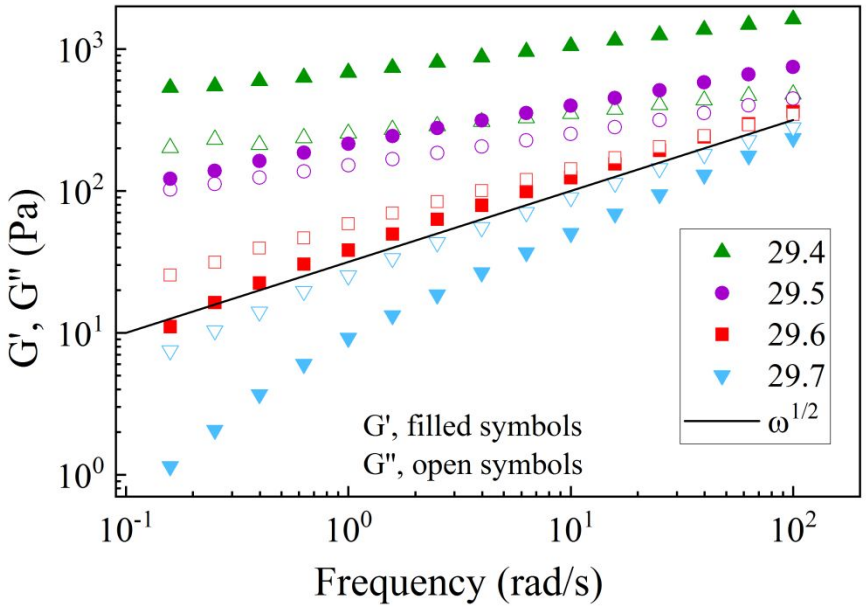

Fig 3 Small angle frequency sweeps of the soft glass sample (ϕ=0.46) at temperatures ranging from 29.4°C to 29.7°C. Rheological measurements began 45 minutes after setting the rheometer to the desired temperature following a quench from the liquid state at 40°C to allow the sample to cool and equilibrate at the set temperature. All tests were conducted at 0.1% strain. The critical temperature occurs between 29.5°C and 29.6°C, and the line indicates the expected power law $G' \sim G'' \sim \omega^{1/2}$ at the critical temperature[50]. All subsequent Rheo-SANS aging experiments were conducted at 29.4°C; at this temperature, a soft attraction-driven glass formed.

Aging phenomena were observed in the attraction-driven glass. In the model system selected for this study, short-range attractions are controlled by temperature via a liquid-to-solid transition of the octadecyl brush grafted to the surface of the silica nanoparticle. Specifically, upon quenching the sample from the liquid state, small amplitude oscillatory shear experiments revealed that the storage modulus (G′) increased by approximately four orders of magnitude, consistent with the formation of a soft, attraction-driven glass (Fig. 4). Moreover, G′ continued to increase after the temperature equilibrated, indicating stiffening of the specimen. This continual increase in storage modulus in time is characteristic of rheological aging, which we further probe via structural measurements in the following section. The time evolution of the moduli (Fig.4 inset) are qualitatively similar to that observed in shear-rejuvenated Laponite suspensions and related systems, as reported by Shanin and Joshi [18]. Note that a different behavior is observed for hard-sphere colloidal glasses, where the elastic modulus is time-independent and aging is only evident from the loss modulus decreasing with glass age[10].

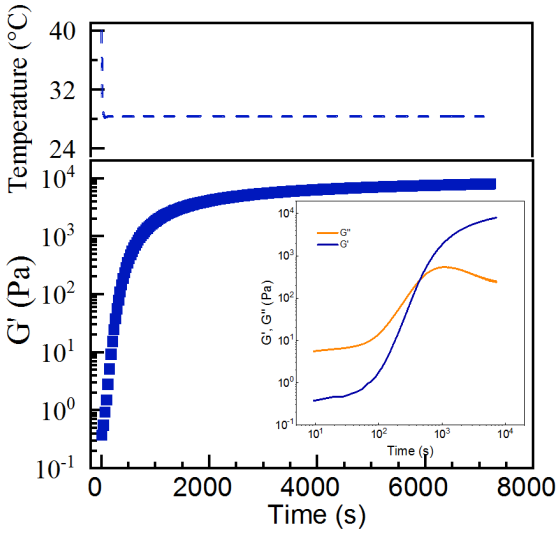

Fig 4 Aging in our model attraction-driven glass. After the glass is quenched from its liquid state, the storage modulus continues to increase over the two-hour experiment, which is indicative of rheological aging. These measurements were conducted at 0.1% strain and a frequency of 1 rad/s using a TA Instruments DHR equipped with a Peltier plate, where we note a 1°C difference in temperature compared to the gas-cooled Rheo-SANS environment used above. The inset shows the evolution of the moduli on a log-log plot.

C. Concurrent Rheological and Structural Measurements

Time-resolved SANS data were collected to monitor the structural evolution of the glass during aging. Samples were immediately quenched from 40°C to the glass state at 29.4°C. Using event mode processing in Igor Pro, the scattering data were binned into 20 intervals, each 6 minutes in duration, and shown in Fig. 5A. Small structural changes are observed in which the greatest changes occur at the longest length scales probes (i.e., lowest q). As shown in Fig. 5, the microstructure evolves to a pattern that would be expected for a concentrated glass. As the sample forms and ages, the evolution in microstructure is consistent with particles sampling progressively lower energy states, in concurrence with the free energy viewpoint of aging. Moreover, as expected, the nearest neighbor peak at $q \approx 0.02$ Å^{-1} corresponds to a length scale of approximately 30 nm, which is the diameter of the particles used in this study. These structural measurements correspond to the rheological experiment conducted above (Fig. 4) and are analyzed jointly below.

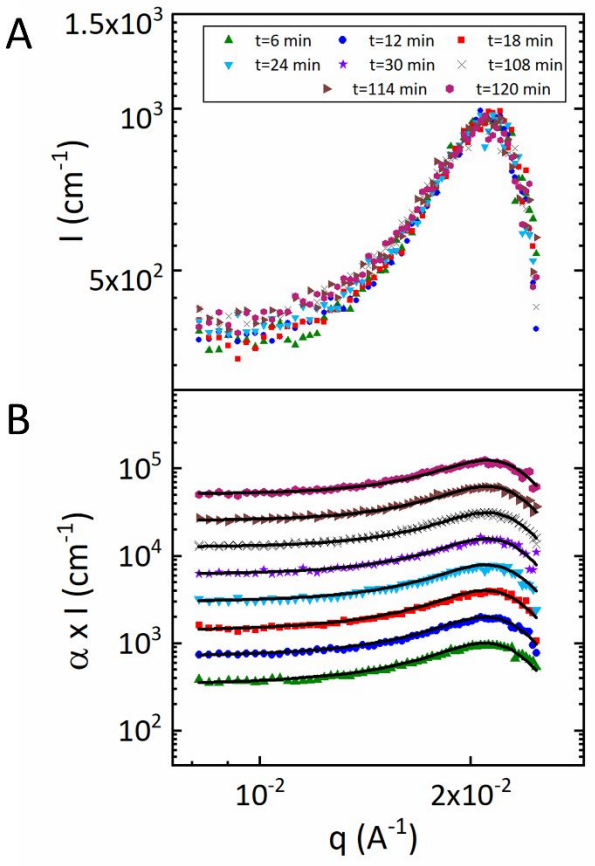

Fig 5 Time-resolved small angle neutron scattering (SANS) data of an AHS glass (ϕ=0.46) during formation and aging. The sample was quenched from its liquid state at 40°C and aged at 29.4°C (i.e., the cooling direction). **A.** Scattering data during the two-hour experiment, which begins with the onset of the quench from 40°C to 29.4°C, were binned into 20 intervals. **B.** The data were fit to the sticky hard sphere model. The intensity was doubled from the previous data set to more clearly display the fits.

Using a structural parameter λ, we directly related rheological aging to structural aging in the thermoreversible model glass. First, to assess structural changes during aging, the scattering data were fit to the SHS model, which is commonly used to model attractive systems [36, 41]. In this work, only one parameter, the Baxter parameter (τ), was adjusted to fit the data at each time point. This τ was used to track the evolution of the microstructure. The data and the fitted models are displayed in Fig. 5B. Note that the intensities at each time point are offset by a factor of two from the previous data set for clarity. For each bin of data, the fitted Baxter parameter τ was obtained, and the evolution of this parameter in time tracks the effective strength of attraction between the particles in the glass as it ages. The Baxter parameters obtained from this analysis represent points along an aging trajectory and are not equilibrium states. To quantify structural changes toward equilibrium, we calculated a structural parameter λ that serves as an order parameter to describe the microstructure as follows:

$$\lambda = \frac{\tau_{40}^{eq} - \tau^{eff}}{\tau_{40}^{eq} - \tau_{\infty}} \quad (1)$$

where τ_{40}^{eq} is the value of the Baxter parameter in the liquid state at 40°C, τ^{eff} is the value of Baxter fit parameter during each time interval and τ_{∞} is the long-time Baxter parameter for this temperature as the sample asymptotically approaches equilibrium. By fitting the SHS model to time-resolved SANS data, τ_{40}^{eq} = 0.367 and $\tau_{\infty} \approx$ 0.281. (Baxter parameters at temperatures of interest are shown in Table 1. Note that τ_{∞} was determined from fitting the last bin of scattering data to the SHS model and was not found by extrapolation.)

The evolution in microstructure and bulk properties are shown in Fig. 6A. The reported G′ values correspond to averaged values of the storage modulus during each 6-minute interval. We note that there is a temperature overshoot (to 28.6°C instead of 29.4°C following a quench from the pre-shear protocol at 40°C) due to imperfect temperature control on the Rheo-SANS equipment that, combined with the high sensitivity of sample to 0.1°C temperature changes (Fig. 3), resulted in the non-monotonic changes in storage modulus early in the experiment. However, after the temperature equilibrated (n.b., deviation from 29.4°C was less than 0.1°C after 34 mins), the modulus of specimen continued to increase throughout the two-hour aging experiment and the long-time aging behavior was not affected by this temperature overshoot during the initial quench. To relate particle interactions to resultant mechanical properties, we first reduce noise from SANS measurements and/or nonlinear model fitting. This is achieved using linear regression to obtain an empirical expression for the structural parameter as a function of the aging time:

$$\lambda = 0.119 \ln t + 0.393 \ , \quad (2)$$

where the units of t are minutes. As the glass ages (t > 30 minutes), there is a monotonic increase in both G′ and λ as the sample evolves towards its equilibrium state. Moreover, Fig. 6B, which displays G′ as a function of λ, indicates that there is a one-to-one relationship between storage modulus and microstructure that evolves in time as the sample ages, similar to colloidal gels [41].

We analyze our results within an Avrami framework to develop an empirical equation that quantitatively captures the relationship between log G′ and λ as the glass ages. The Avrami equation, which is a kinetic model that describes the process of crystallization by nucleation and growth, was previously used to relate the mechanical properties to a space filling parameter, ζ, during crystallization of a fatty acid model system [51]. In this spirit, we adapt the Avrami analysis to relate the mechanical properties (G′) to the underlying microstructure (λ) as the glass ages:

$$\log G' = 3.40 \left(1 - \exp\left(-7.64\, \lambda^{10.92}\right)\right), \quad (3)$$

where 0.80<λ<0.96. Fig. 6B shows this empirical equation represents the data well. However, based on this analysis, there is no clear interpretation for the Avrami parameters in the above

equation. Further work is required to interpret the results within the Avrami framework and extract a physical meaning. Importantly, however, this is the first approach toward developing a phenomenological relationship between colloidal glass microstructure and rheological properties during glass aging. Moreover, the monotonic increase in both the bulk properties and structural parameter is consistent with the free energy landscape viewpoint of aging, in which a sample evolves toward equilibrium by sampling progressively lower energy states.

Table 1 Table of Baxter parameters used in this work.

Temperature (°C)	τ value
40°C	$\tau_{40}^{eq} = 0.367$
25°C	$\tau_{25}^{eq} = 0.234$
29.4°C	$\tau_{\infty} \approx 0.281$

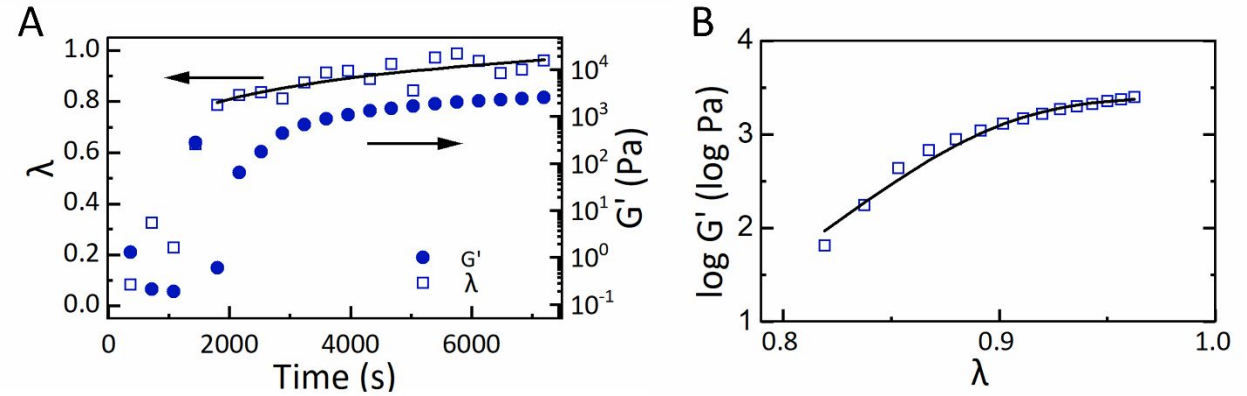

Fig 6 A quantitative relationship between the bulk property changes (G′) and the underlying microstructure (λ) during colloidal glass aging. **A.** The evolution in G′ and λ are shown. Noise from SANS measurements and/or nonlinear model fitting was reduced by using linear regression to obtain expressions for the effective τ as a function of the aging time: λ= 0.119 ln t + 0.393 where t is given in minutes. As the glass ages (t > 30 minutes), there is a monotonic increase in both G′ and λ as the sample evolves towards its equilibrium state. The variation in data points before 2000 s is due to imperfect temperature control in cooling to 29.4°C. **B.** G′ is plotted as a function of λ. A specific storage modulus corresponds to a specific microstructure, which evolve in time as the sample ages. The Avrami equation (solid line, eqn 3) captures the relationship between log G′ and λ as the glass ages.

While the above analysis enabled development of a quantitative, but empirical relationship between structural and rheological aging in colloidal glasses, the mechanistic origin of the aging process remains unclear. To understand this process, we calculate a localization length based on predictions from mode coupling theory (MCT). The localization length is the mean squared

displacement of particle motion when trapped within a cage of nearest neighbors. The prediction from MCT is shown below:

$$\frac{G'a^3}{k_BT} = 0.29\frac{\phi a^2}{r_{loc}^2}\ , \tag{4}$$

where a is the particle radius and r_{loc} is the localization length [52]. Using the final G′ value measured after two hours of aging during the small amplitude oscillatory shear measurement shown in Fig. 4, a localization length of 3.8 nm was calculated. This localization length is very close to the localization length of 3.3 nm calculated for the AHS gel [41]. Moreover, the calculated localization length is on the order of the brush size, which was reported as 2.76 nm by Eberle and coworkers [40], who proposed interdigitation of the brush layer as the aging mechanism in the system [36]. This result suggests local particle motion as the mechanism of aging in this system, which is similar to what was observed in colloidal gels. Overall, the localization length calculated from MCT suggests that local particle rearrangements occurring persistently within the glass are responsible for the observed structural and rheological aging.

a. Effect of Thermal History

To evaluate the effect of thermal history on the evolution of bulk properties and microstructure, the glass was formed using two distinct thermal profiles. As described in the methods section, samples were formed by: (1) quenching from 40°C to 29.4°C (the cooling direction) or (2) quenching from 40°C to 25°C to 29.4°C (the heating direction). Thus far, all samples were formed following application of the cooling profile. Here, we evaluate the microstructure and bulk properties from an alternative thermal path, designated here as the heating direction, and compare them to the results presented earlier for samples quenched from the cooling profile. To track the structural evolution of the glass, time-resolved SANS data were collected. Specifically, samples were rejuvenated by following the pre-shear protocol at 40°C and quenched to 25°C for 45 minutes to provide additional equilibration time following the temperature controller reaching the set point. The temperature was raised from 25°C to 29.4°C and Fig. 7 displays the corresponding evolution in microstructure as the AHS colloidal glass forms and ages from the heating direction. Similar to the cooling-direction aging experiments, the heating-direction aging data was analyzed using event mode processing in Igor Pro, in which the scattering data was binned into 20 intervals, 6 minutes each in duration. The scattering data corresponding to samples formed and aged from the heating profile are consistent with a more deeply quenched glass that transitions to a less attractive glass and evolves towards an equilibrium state. In contrast to the cooling data, the glasses formed and aged from the heating direction appear to sample fewer energy states, which is consistent with particles escaping from local free energy minima which leads to the system subsequently sampling lower energy via thermal motion as the glass ages. These results qualitatively mirror the behavior observed for AHS colloidal gels [41] and support aging as a trajectory in the free energy landscape where the microstructure evolves towards an equilibrium state characterized by increasing particle attractions.

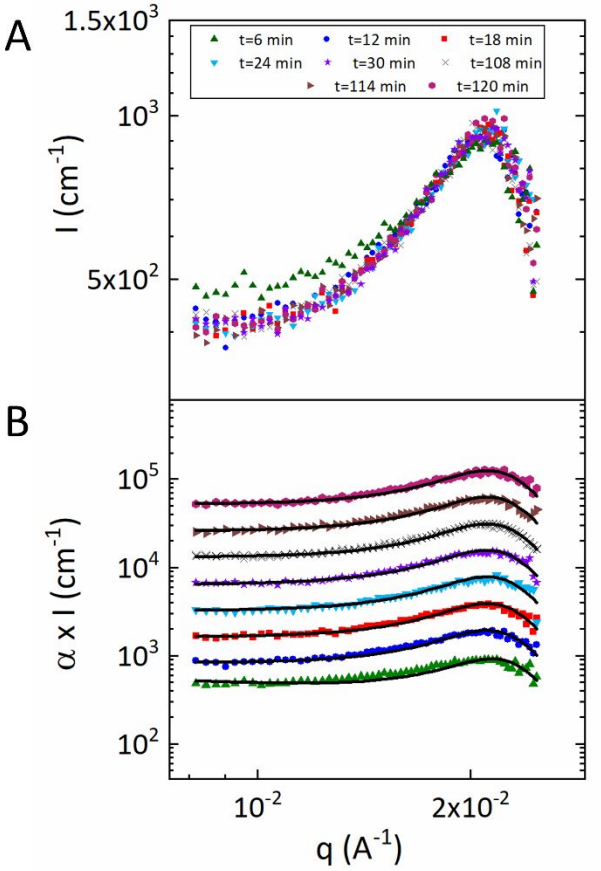

Fig 7 Time-resolved small angle neutron scattering (SANS) data of an AHS glass (ϕ=0.46) during formation and aging. The samples were initially quenched from its liquid state at 40°C to 25°C and aged at 29.4°C (i.e., the heating direction). **A.** Scattering data during the two-hour experiment (including the approach from 25°C to 29.4°) were binned into 20 intervals. **B.** The data were fit to the sticky hard sphere (SHS) model to obtain a single structural parameter, λ, to quantify the structural aging in the glass. The intensity was doubled from the previous data set to more clearly display the fits.

The influence of the thermal history on the mechanical properties and microstructure is shown in Fig. 8A. While the path towards the equilibrium state of the glass is highly dependent on the quenching profile, samples formed and aged from both quenched profiles appear to approach the same aged state. For this analysis, once again, we reduce noise from SANS measurements and/or nonlinear model fitting via linear regression as shown by the solid lines on the plot. Importantly, for both thermal histories, a monotonic increase in bulk properties, which correspond to a monotonic evolution in microstructure, was observed during aging. In specimens formed from both thermal profiles, the data suggests a one-to-one correspondence between rheological aging and structural aging, which is consistent with aging as a trajectory in the free energy landscape, in which the glass evolves towards lower energy states as it approaches its equilibrium state. To evaluate how thermal history impacts the aging trajectory, the mechanical properties are shown as function of the structural parameter in Fig. 8B. The error bars represent the 95% confidence interval on the regressed structural parameter. Using this

analysis for an aging AHS gel, we observed a one-to-one correspondence between mechanical properties (G′) and gel microstructure (λ) during aging, which was independent of the thermal pathway [41]. Interestingly, for AHS colloidal glasses, it appears that the relationship between G′ and λ during aging may be influenced by the thermal profile. It is important to note that both gel and glass aging were monitored over a two-hour period, yet particle rearrangements were likely slower in the concentrated sample due to the reduced mobility. In the aging gel sample, the convergence of G′ from the heating and cooling direction occurred after approximately an hour, after which the thermal history did not affect the relationship between G′ and λ; meanwhile, the convergence of the storage moduli in the glass sample occurred near the very end of the two hour experiment as displayed in Fig. 8A. It is at these later time points that values begin to converge as shown in Fig. 8B. Based on these results, we hypothesize that the influence of the thermal profile during formation may weaken as the sample ages, and a longer aging experiment may reveal a convergence of two thermal profiles shown in Fig. 8B.

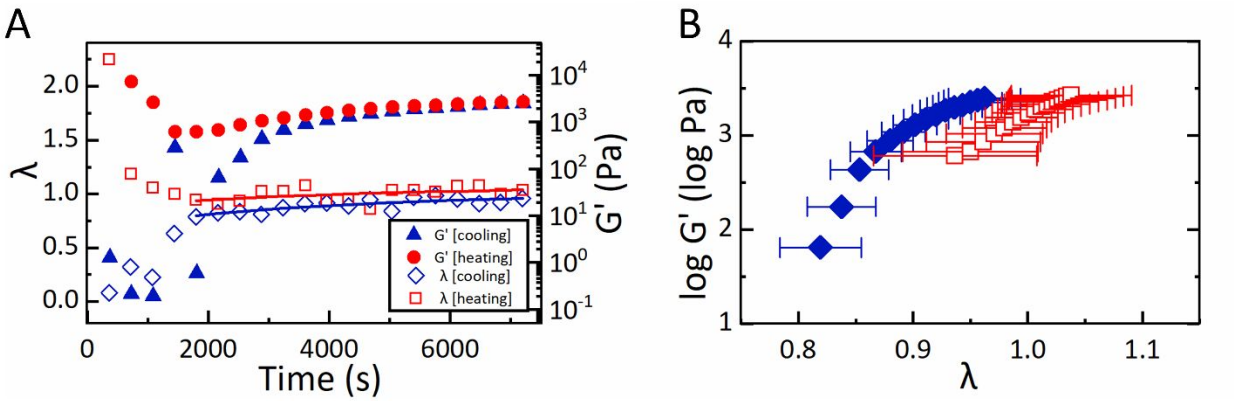

Fig 8 The influence of thermal history on the microstructure and bulk properties during aging. **A.** The evolution of the structural parameter λ and storage modulus, reported every six minutes, over a two-hour aging experiment is shown for a ϕ=0.46 colloidal glass. Glasses were formed and aged from two distinct thermal profiles: (1) the cooling profile in which the temperature was dropped from 40°C to 29.4°C and (2) the heating profile where the temperature was increased from 25°C to 29.4°C following a pre-shear protocol at 40°C. **B.** The storage modulus is plotted as a function of its microstructure, captured by the regressed structural parameter λ, which indicates that the relationship between G′ and λ during aging may be influenced by the thermal profile.

b. Effect of Shear History

To assess how processing conditions influence the aging process, we probed the aged glass by applying shear. In these experiments, glasses were formed from the cooling profile and aged to a reference state of 4250 s, which was selected for consistency to prior work [41]. The aged sample was then immediately sheared at rates of 5 s^{-1}, 100 s^{-1}, 500 s^{-1} or 1000 $s^{-1}$for 20 minutes. The same sample was used for this set of experiments, and was fully rejuvenated via thermal cycling between tests, as described in the methods section. The microstructure and corresponding viscosity during shear are displayed in Fig. 9A and Fig. 9B, respectively. Similar to the previous

analysis described above, the data from the microstructural measurements were fit to the SHS model, which enabled the calculation of λ. For shear rates of 5 s^{-1}, 100 s^{-1}, 500 s^{-1} and 1000 s^{-1}, structural parameters of 1.02±0.03, 1.27±0.03, 1.08±0.03 and 0.93±0.03 were calculated, respectively. The increase and subsequent decrease in λ is consistent with the shear-induced building and destruction of the sample microstructure, respectively. These results are similar to the experimental results of Eberle and co-workers, which showed that large strains (comparable to or exceeding the interparticle force) destroyed the sample microstructure while weak flow led to additional structuring of the sample [53]. Under the conditions studied in this work, the pronounced shear-induced anisotropy measured by Eberle et al. was not observed. It is important to note that the scattering experiments in Fig. 9A probe local structure while the viscosity measurements in Fig. 9B reflect the global sample under shear. Thus, when the shear rate of 100 s^{-1} is applied, these results signify restructuring at smaller length scales during the shear-induced breakage of the glass sample, which results in a flowing sample. These measurements are consistent with flowing particle clusters in which the particles become more closely associated under shear. Thus, the changes in λ observed here indicate shear-induced structural changes, which do not persist following the cessation of shear, as discussed below.

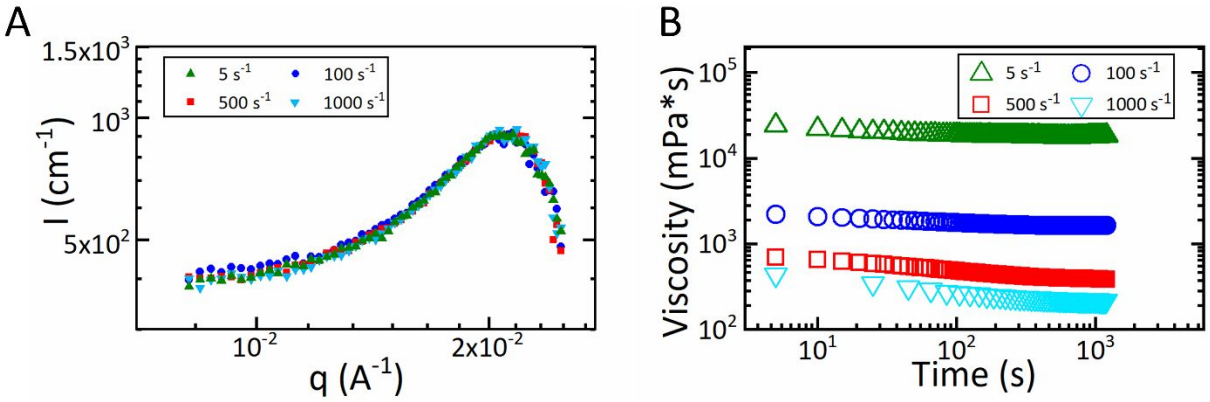

Fig 9 Response of the aged colloidal glass during shear. **A.** Microstructural measurements of 0.46 volume fraction colloidal glass under shear rates of 5 s^{-1}, 100 s^{-1}, 500 s^{-1} and 1000 s^{-1} for 20 minutes are shown. The corresponding λ values are: $\lambda_{5s^{-1}}$ =1.02±0.03, $\lambda_{100s^{-1}}$ =1.27±0.03, $\lambda_{500s^{-1}}$ =1.08±0.03 and $\lambda_{1000s^{-1}}$=0.93±0.03. **B.** The corresponding viscosity measurements during shear are also displayed.

Following the application of shear, the aging process was tracked for an additional 4250 s to further assess the influence of shear on the aging trajectory. Specifically, the continued aging of the specimen was monitored using small amplitude oscillatory shear measurements. The evolution of the microstructure is displayed in Fig. 10A after shearing at 1000 s^{-1}. An initial, intermediate and final structure is shown and the corresponding λ values increase from 0.64±0.05 to 0.95±0.05 by the conclusion of the 4250 s aging experiment. The increasing λ values signify the rebuilding of structure as the sample ages. Fig. 10B displays the corresponding mechanical property changes following shearing at the specified rate. Immediately following shear, G′ values decrease to below the detection limit on the rheometer following shearing at 500 s^{-1} and 1000 s^{-1}, indicating the higher shear rates rejuvenated the sample's mechanical properties. The

mechanical properties following shearing at 100 s^{-1} show an order of magnitude decrease of G′, yet does not appear to fully restore the mechanical properties, while the bulk properties following shearing at 5 s^{-1} show only a slight decrease in mechanical properties immediately following shear compared to the samples sheared at higher rates. At the lowest shear rate tested (5 s^{-1}), we do not observe clear evidence of overaging. We note that the sample sheared at 5 s^{-1} evolved to a slightly higher storage modulus at the conclusion of the experiment when compared to samples that were sheared at higher rates. However, this difference may also be due to slight variability in aging (inset in Fig. 10B). At the higher shear rates tested, the rejuvenation of mechanical properties indicates that shear destroys the microstructure, decreasing the glass "age". However, despite rejuvenation of bulk properties following shear, the underlying microstructure may only partially rejuvenate, as discussed further below. Regardless of shear history, however, the samples eventually evolve along a similar trajectory as the sample ages (Fig. 10B).

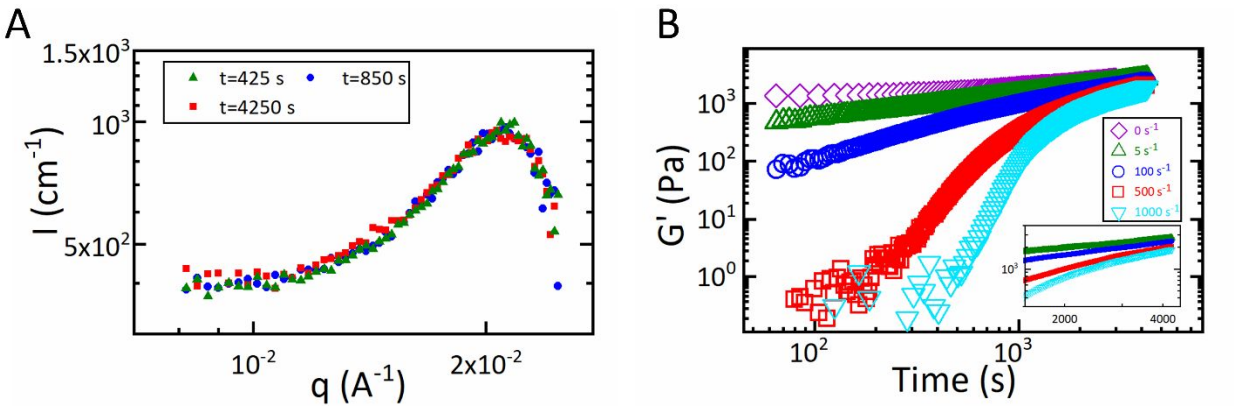

Fig 10 Response of the aged colloidal glass following shear. **A.** Time-resolved microstructural measurements following 20 minutes of shearing at a rate of 1000 s^{-1} (λ_{425s}=0.64±0.05, λ_{850s}=0.74±0.05, λ_{4250s}=0.95±0.05). **B.** The evolution of mechanical properties under SAOS after shearing for 20 minutes at the specified shear rate is shown. The inset shows a close-up view of the evolution of G′ at long-times.

The effectiveness of mechanical rejuvenation to restore the original microstructure in colloidal glasses has been not yet been extensively investigated. By using a system that is fully rejuvenated by thermal cycling, we investigate the use of shear as a rejuvenation method, which may restore the original mechanical properties, but incompletely rejuvenate the microstructure. Fig. 11A and B compare the effects of thermal rejuvenation and mechanical rejuvenation on the evolution of mechanical properties and microstructure, respectively. Thermal rejuvenation consisted of shearing the sample at 10 s^{-1} in its liquid state at 40°C for 10 minutes followed by holding the sample quiescently at 40°C for 2 minutes prior to aging at 29.4°C. Mechanical rejuvenation consisted of shearing the sample at isothermally (at 29.4°C) at 1000 s^{-1} for 20 minutes prior to aging at 29.4°C. Following the cessation of shear, an immediate rise in the mechanical properties was observed, whereas the sample that was thermally rejuvenated evolved

more slowly. This indicates that either the glass structure was not completely erased by shearing, or that the microstructure continued to evolve under shear. Fig. 11B confirms the former perspective as the sheared sample starts with a much larger value of λ. This observation is significant because many investigators use shear rejuvenation for hard-sphere glasses [10] as well as gels and glasses formed by depletion attractions, such as in colloid-polymer mixtures [23], as they cannot use thermal cycling. Our work presented here suggests that one must using caution when assuming that shear is sufficient to fully rejuvenate the microstructure based only on the mechanical properties.

Despite differences in the trajectory during formation and early aging, the samples appear to tend toward a similar aged state regardless of shear history. Similar aging trajectories for both thermal and mechanical rejuvenation are shown in Fig. 12; note that the cooling data were shifted in time only (by 24 minutes). This long-time behavior is qualitatively similar to the results obtained for colloidal gels [41]. Indeed, the same empirical relationship between G′ and λ that was developed for glass aging following a thermal quench (equation 3) applies to glass aging following shear at the rates tested in this work (Fig. 13). We note that at short times immediately following shear (corresponding to low λ values in the figure), the data deviates from the relationship, which indicates that immediately following shear, λ may not fully characterize the microstructure. However, during long-time aging, this result indicates that there is a one-to-one correspondence between the mechanical properties and underlying microstructure under these experimental conditions.

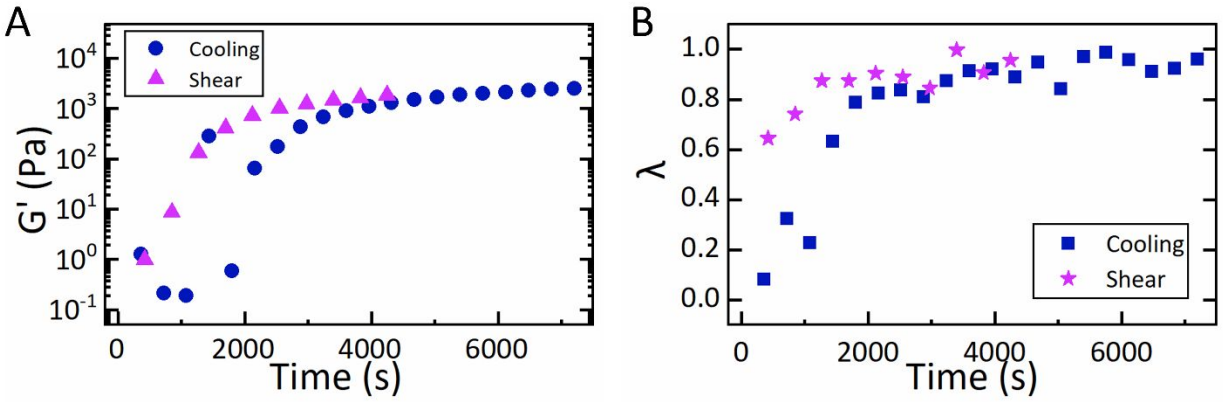

Fig 11 The effects of thermal and mechanical rejuvenation on gel mechanical properties (G′) and microstructure (λ) during aging. Thermal rejuvenation consisted of shearing the sample at 10 s^{-1} in its liquid state at 40°C for 10 minutes followed by holding the sample quiescently at 40°C for 2 minutes prior to aging at 29.4°C. Mechanical rejuvenation consisted of shearing the sample at isothermally (at 29.4°C) at 1000 s^{-1} for 20 minutes prior to aging at 29.4°C. **A.** The evolution of storage modulus following thermal cycling and shear is shown. **B.** The evolution of microstructure following thermal cycling and shear is shown.

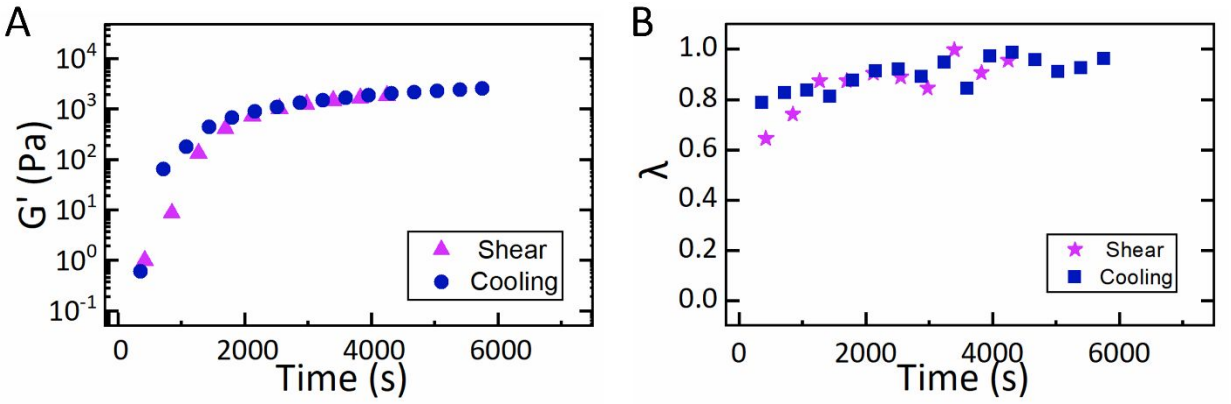

Fig 12 Data from Fig 11 replotted to directly compare thermal rejuvenation to shear rejuvenation. Cooling data were shifted in time only (by 24 minutes) to overlay the aging trajectory following shear rejuvenation.

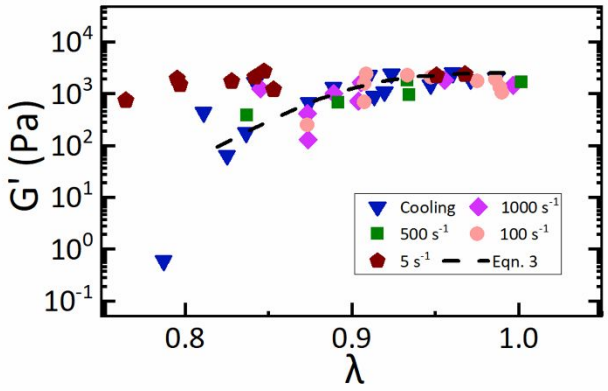

Fig 13 Storage moduli plotted as a function of microstructure (λ) following shear. The same relationship between G′ and λ that was developed for glass aging following a thermal quench (Eqn. 3, dashed black line) applies to glass aging following shearing the sample at 5 s^{-1}, 100 s^{-1}, 500 s^{-1} and 1000 s^{-1}, indicating that there is a one-to-one correspondence between the mechanical properties and underlying microstructure under these experimental conditions. We note that at short times immediately following shear (corresponding to low λ values in the figure), the data deviates from the relationship, which indicates that immediately following shear, λ may not fully characterize the microstructure.

The rejuvenation, or reversal of aging, via application of temperature and shear stress for the thermoversible colloidal glass can be analyzed in the context of related literature. The structural and mechanical measurements conducted here offer additional experimental evidence that suggests discrepancies between thermal and mechanical rejuvenation, generally supporting earlier experimental findings for polymers [18, 54, 55]. Molecular simulations offer an explanation for these observations and reveal that the potential energy landscape is altered upon application of shear strain, which causes the disappearance of local minima and barrier heights, leading the system to toward an alternative energy minimum[56]. The simulations show that for their system, high strain rates ($\gamma \sim 10^{12}$ s^{-1}) are required for the strain-activated contribution of diffusion to be as significant as the thermal contribution [56]. Perhaps this alteration in the potential energy landscape gives rise to the differences in the structural parameter λ when thermal and shear rejuvenations protocols are compared in Figures 11-13. The structural differences resulting from

comparing thermal to mechanical perturbations observed here are also noted in other studies of aging colloidal systems[18, 55, 57]. In the study by Purnomo et al., differences in G' are noted when mechanical and thermal rejuvenation are compared, and the authors suggest that both protocols erase sample memory but lead to different initial states. In the system probed here, our results suggest that shear may incompletely erase the sample's structure, thus leading to initial differences in mechanical properties. Overall, our results contribute further evidence of discrepancies between thermal and mechanical rejuvenation by directly and simultaneously measuring structural and mechanical changes via Rheo-SANS.

IV. Summary and Conclusions

In this work, rheological aging and structural aging in a thermoreversible colloidal glass (attractive driven, ϕ=0.46) were quantitatively related using concurrent rheometry and time-resolved small angle neutron scattering (Rheo-SANS) measurements. Data from time-resolved SANS measurements were fit to the SHS model to obtain a Baxter parameter at each time-point, and a microstructural order parameter λ was calculated to quantify the evolution in microstructure as the system ages. A monotonic increase in both the bulk properties and structural parameter during aging was observed, from which an empirical, Avrami-like relationship between G′ and λ was established. To our knowledge, this is the first approach toward developing a phenomenological relationship between colloidal glass microstructure and rheological properties during aging. Mode coupling theory [52] predicts a localization length of 3.8 nm for this AHS glass, which is on the order of the brush size, indicating that local particle rearrangements may be responsible for the observed rheological aging. We note that similar behavior has been reported for aging in thermoreversible gels of the same colloidal particles [41].

By probing the system with different thermal profiles and shear rates, the effects of thermal and shear history on glass mechanical properties and microstructure during aging were investigated. At the shear rates tested, shear disrupts the glass microstructure, decreasing the glass "age" and either incompletely or fully rejuvenating the mechanical properties at lower (5 s^{-1} and 100 s^{-1}) and higher (500 s^{-1} and 1000 s^{-1}) shear rates, respectively. As the model system employed in this study is fully rejuvenated by thermal cycling, we directly compared thermal rejuvenation to mechanical rejuvenation. After mechanical rejuvenation, the evolution of the storage modulus and microstructural order parameter λ progressed more rapidly compared to the thermal rejuvenation, indicating that either the glass structure may not be completely erased by shear or that the microstructure continues to evolve under shear. Thus, despite rejuvenation of bulk properties following shear, the underlying microstructure may only partially rejuvenate as there may be residual stresses [24]. Nonetheless, while the glass formation and aging trajectory is significantly affected immediately following a temperature quench or the application of stress, the samples evolve along a common aging trajectory, independent of the thermal and shear histories tested in this work, at long times. Thus, despite differences in processing conditions tested here, all samples eventually age similarly, suggesting a trajectory towards a common equilibrium state.

In conclusion, this work extends the understanding of aging behavior in colloidal glasses by quantitatively linking the macroscopic bulk property changes to the underlying microstructural rearrangements. The results and analysis contained herein may be applied to further understand the molecular mechanism underlying the aging process in other model colloidal systems or colloidal-based consumer products. In particular, this microstructural ageing is distinct from chemical ageing in reacting systems, also described as contact aging [58]. Moreover, our measurements and approach may be employed to validate or improve simulations, as well as be extended to examine and interpret non-equilibrium behavior in atomic or molecular systems. For example, recent work on relating vitrification in soft colloidal pastes to excess entropy, which is cast in terms of the pair distribution function, may intriguingly provide another method of connecting the microstructural evolution observed here to the mechanical properties [59].

Conflicts of Interest

There are no conflicts of interest to declare.

Acknowledgements

The authors thank Ms. Rong Song for assistance with the graphics for this manuscript. This manuscript was prepared under cooperative agreements #370NANB17H302 and 70NANB15H260 from NIST, U.S. Department of Commerce. We acknowledge the support of the National Institute of Standards and Technology, U.S. Department of Commerce, in providing the neutron research facilities used in this work. This work utilized facilities supported in part by the National Science Foundation under Agreement No. DMR-0944772. The statements, findings, conclusions and recommendations are those of the authors and do not necessarily reflect the view of NIST or the U.S. Department of Commerce. We also acknowledge Lafayette College for financial support through an ARC grant.

V. References

1. *Basic Energy Sciences Advisory Committee Report, U.S. Department of Energy*, 2007.
2. Y. M. Joshi, *Annu Rev Chem Biomol*, 2014, **5**, 181-202.
3. P. J. Lu and D. A. Weitz, *Annu Rev Conden Ma P*, 2013, **4**, 217-233.
4. R. P. A. Dullens, D. Aarts and W. K. Kegel, *Proceedings of the National Academy of Sciences of the United States of America*, 2006, **103**, 529-531.
5. R. Pandey, M. Spannuth and J. C. Conrad, *JoVE*, 2014, DOI: doi:10.3791/51461, e51461.
6. B. Abou, D. Bonn and J. Meunier, *Phys Rev E*, 2001, **64**.
7. Y. M. Joshi and G. Petekidis, *Rheologica Acta*, 2018, **57**, 521-549.
8. G. Petekidis and N. J. Wagner, in *Theory and Applications of Colloidal Suspension Rheology*, eds. N. J. Wagner and J. Mewis, Cambridge University Press, Cambridge UK, 2021, DOI: 10.1017/9781108423038, ch. 6, pp. 173-226.
9. L. Cipelletti and L. Ramos, *J Phys-Condens Mat*, 2005, **17**, R253-R285.
10. A. R. Jacob, E. Moghimi and G. Petekidis, *Physics of Fluids*, 2019, **31**, 087103.
11. L. Cipelletti and L. Ramos, *Curr Opin Colloid In*, 2002, **7**, 228-234.
12. H. Y. Guo, S. Ramakrishnan, J. L. Harden and R. L. Leheny, *J Chem Phys*, 2011, **135**.
13. G. Petekidis, *J Rheol*, 2014, **58**, 1085-1087.
14. B. Abou and F. Gallet, *Phys Rev Lett*, 2004, **93**.
15. D. Bonn, S. Tanase, B. Abou, H. Tanaka and J. Meunier, *Phys Rev Lett*, 2002, **89**.
16. Y. M. Joshi and G. R. K. Reddy, *Phys Rev E*, 2008, **77**.
17. R. Bandyopadhyay, P. H. Mohan and Y. M. Joshi, *Soft Matter*, 2010, **6**, 1462-1466.
18. A. Shahin and Y. M. Joshi, *Langmuir*, 2010, **26**, 4219-4225.
19. B. M. Erwin, D. Vlassopoulos and M. Cloitre, *J Rheol*, 2010, **54**, 915-939.
20. S. A. Rogers, D. Vlassopoulos and P. T. Callaghan, *Phys Rev Lett*, 2008, **100**.
21. K. N. Pham, S. U. Egelhaaf, P. N. Pusey and W. C. K. Poon, *Phys Rev E*, 2004, **69**.
22. K. N. Pham, G. Petekidis, D. Vlassopoulos, S. U. Egelhaaf, W. C. K. Poon and P. N. Pusey, *J Rheol*, 2008, **52**, 649-676.
23. N. Koumakis and G. Petekidis, *Soft Matter*, 2011, **7**, 2456-2470.
24. M. Ballauff, J. M. Brader, S. U. Egelhaaf, M. Fuchs, J. Horbach, N. Koumakis, M. Krüger, M. Laurati, K. J. Mutch, G. Petekidis, M. Siebenbürger, T. Voigtmann and J. Zausch, *Phys Rev Lett*, 2013, **110**, 215701.
25. E. Stiakakis, A. Wilk, J. Kohlbrecher, D. Vlassopoulos and G. Petekidis, *Phys Rev E*, 2010, **81**.
26. G. C. Cianci, R. E. Courtland and E. R. Weeks, *Solid State Commun*, 2006, **139**, 599-604.
27. A. M. Puertas, M. Fuchs and M. E. Cates, *Phys Rev E*, 2007, **75**.
28. C. P. Royall, S. R. Williams, T. Ohtsuka and H. Tanaka, *Nat Mater*, 2008, **7**, 556-561.
29. S. Jabbari-Farouji, G. H. Wegdam and D. Bonn, *Phys Rev Lett*, 2007, **99**.
30. P. Sollich, F. Lequeux, P. Hebraud and M. E. Cates, *Phys Rev Lett*, 1997, **78**, 2020-2023.
31. V. Viasnoff and F. Lequeux, *Phys Rev Lett*, 2002, **89**.
32. D. J. Lacks and M. J. Osborne, *Phys Rev Lett*, 2004, **93**.
33. N. Koumakis, M. Laurati, A. R. Jacob, K. J. Mutch, A. Abdellali, A. B. Schofield, S. U. Egelhaaf, J. F. Brady and G. Petekidis, *J Rheol*, 2016, **60**, 603-623.
34. A. P. R. Eberle and L. Porcar, *Curr Opin Colloid In*, 2012, **17**, 33-43.
35. G. B. McKenna, *J Phys-Condens Mat*, 2003, **15**, S737-S763.
36. A. P. R. Eberle, R. Castaneda-Priego, J. M. Kim and N. J. Wagner, *Langmuir*, 2012, **28**, 1866-1878.

37. A. P. R. Eberle, N. J. Wagner and R. Castaneda-Priego, *Phys Rev Lett*, 2011, **106**.
38. J. M. Kim, J. Fang, A. P. R. Eberle, R. Castaneda-Priego and N. J. Wagner, *Phys Rev Lett*, 2013, **110**.
39. J. M. Kim, A. P. R. Eberle, A. K. Gurnon, L. Porcar and N. J. Wagner, *J Rheol*, 2014, **58**, 1301-1328.
40. A. P. R. Eberle, N. J. Wagner, B. Akgun and S. K. Satija, *Langmuir*, 2010, **26**, 3003-3007.
41. M. B. Gordon, C. J. Kloxin and N. J. Wagner, *J Rheol*, 2017, **61**, 23-34.
42. A. K. Vanhelden, J. W. Jansen and A. Vrij, *J Colloid Interf Sci*, 1981, **81**, 354-368.
43. L. Porcar, D. Pozzo, G. Langenbucher, J. Moyer and P. D. Butler, *Review of Scientific Instruments*, 2011, **82**, 083902.
44. S. R. Kline, *J Appl Crystallogr*, 2006, **39**, 895-900.
45. L. J. Kaufman and D. A. Weitz, *The Journal of Chemical Physics*, 2006, **125**, 074716.
46. N. E. Valadez-Perez, Y. Liu, A. P. R. Eberle, N. J. Wagner and R. Castaneda-Priego, *Phys Rev E*, 2013, **88**.
47. E. Zaccarelli, *Journal of Physics: Condensed Matter*, 2007, **19**, 323101.
48. J. Bergenholtz and M. Fuchs, *Physical Review E*, 1999, **59**, 5706-5715.
49. K. N. Pham, A. M. Puertas, J. Bergenholtz, S. U. Egelhaaf, A. Moussaid, P. N. Pusey, A. B. Schofield, M. E. Cates, M. Fuchs and W. C. K. Poon, *Science*, 2002, **296**, 104-106.
50. F. Chambon and H. H. Winter, *J. Rheol.*, 1987, **31**, 683-697.
51. C. B. Street, Y. Yarovoy, N. J. Wagner, M. S. Vethamuthu, K. D. Hermanson and K. P. Ananthapadmanabhan, *Colloid Surface A*, 2012, **406**, 13-23.
52. Y. L. Chen and K. S. Schweizer, *J Chem Phys*, 2004, **120**, 7212-7222.
53. A. P. R. Eberle, N. Martys, L. Porcar, S. R. Kline, W. L. George, J. M. Kim, P. D. Butler and N. J. Wagner, *Phys Rev E*, 2014, **89**.
54. G. B. McKenna, *Journal of Physics: Condensed Matter*, 2003, **15**, S737-S763.
55. X. Peng and G. B. McKenna, *Phys Rev E*, 2014, **90**, 050301.
56. M. M. Frey and D. J. Lacks, *The Journal of Chemical Physics*, 2000, **112**, 2909-2915.
57. E. H. Purnomo, D. v. d. Ende, J. Mellema and F. Mugele, *Europhysics Letters (EPL)*, 2006, **76**, 74-80.
58. F. Bonacci, X. Chateau, E. M. Furst, J. Fusier, J. Goyon and A. Lemaître, *Nat Mater*, 2020, DOI: 10.1038/s41563-020-0624-9.
59. R. T. Bonnecaze, F. Khabaz, L. Mohan and M. Cloitre, *J Rheol*, 2020, **64**, 423-431.

Structural and Rheological Aging in Model Attraction-Driven Glasses by Rheo-SANS

We develop a quantitative relationship between macroscopic properties and underlying microstructure during colloidal glass aging using rheology and neutron scattering.